biosensors

MDPI

Article

Novel Amperometric Biosensor Based on Tyrosinase/Chitosan Nanoparticles for Sensitive and Interference-Free Detection of Total Catecholamine

Valeria Gigli [1], Cristina Tortolini [1], Eliana Capecchi [2], Antonio Angeloni [1], Andrea Lenzi [1] and Riccarda Antiochia [3,*]

[1] Department of Experimental Medicine, Sapienza University of Rome, Viale Regina Elena 324, 00166 Rome, Italy; valeria.gigli@uniroma1.it (V.G.); cristina.tortolini@uniroma1.it (C.T.); antonio.angeloni@uniroma1.it (A.A.); andrea.lenzi@uniroma1.it (A.L.)
[2] Department of Biological and Ecological Sciences, University of Tuscia, 01100 Viterbo, Italy; e.capecchi@unitus.it
[3] Department of Chemistry and Drug Technologies, Sapienza University of Rome, Piazzale Aldo Moro 5, 00185 Rome, Italy
* Correspondence: riccarda.antiochia@uniroma1.it

Abstract: The regulation of nervous and cardiovascular systems and some brain-related behaviors, such as stress, panic, anxiety, and depression, are strictly dependent on the levels of the main catecholamines of clinical interest, dopamine (DA), epinephrine (EP), and norepinephrine (NEP). Therefore, there is an urgent need for a reliable sensing device able to accurately monitor them in biological fluids for early diagnosis of the diseases related to their abnormal levels. In this paper, we present the first tyrosinase (Tyr)-based biosensor based on chitosan nanoparticles (ChitNPs) for total catecholamine (CA) detection in human urine samples. ChitNPs were synthetized according to an ionic gelation process and successively characterized by SEM and EDX techniques. The screen-printed graphene electrode was prepared by a two-step drop-casting method of: (i) ChitNPS; and (ii) Tyr enzyme. Optimization of the electrochemical platform was performed in terms of the loading method of Tyr on ChitNPs (nanoprecipitation and layer-by-layer), enzyme concentration, and enzyme immobilization with and without 1-ethyl-3-(3-dimethylaminopropyl)-carbodiimide (EDC) and N-hydroxysuccinimide (NHS) as cross-linking agents. The Tyr/EDC-NHS/ChitNPs nanocomposite showed good conductivity and biocompatibility with Tyr enzyme, as evidenced by its high biocatalytic activity toward the oxidation of DA, EP, and NEP to the relative o-quinone derivatives electrochemically reduced at the modified electrode. The resulting Tyr/EDC-NHS/ChitNPs-based biosensor performs interference-free total catecholamine detection, expressed as a DA concentration, with a very low LOD of 0.17 μM, an excellent sensitivity of 0.583 μA μM^{-1} cm^{-2}, good stability, and a fast response time (3 s). The performance of the biosensor was successively assessed in human urine samples, showing satisfactory results and, thus, demonstrating the feasibility of the proposed biosensor for analyzing total CA in physiological samples.

Keywords: total catecholamine; tyrosinase; chitosan nanoparticles; amperometric biosensor; graphene screen-printed electrode

Citation: Gigli, V.; Tortolini, C.; Capecchi, E.; Angeloni, A.; Lenzi, A.; Antiochia, R. Novel Amperometric Biosensor Based on Tyrosinase/Chitosan Nanoparticles for Sensitive and Interference-Free Detection of Total Catecholamine. *Biosensors* **2022**, *12*, 519. https://doi.org/10.3390/bios12070519

Received: 27 June 2022
Accepted: 9 July 2022
Published: 12 July 2022

1. Introduction

Catecholamines (Cas) are both neurotransmitters and hormones that play fundamental roles in central nervous and cardiovascular systems [1–3]. High CA levels, in particular dopamine (DA), epinephrine (EP), and norepinephrine (NEP), indicate cardiotoxicity leading to tachycardia and heart failure [4]. In contrast, low levels of CA are responsible for several neurological diseases, such as Parkinson's disease, Alzheimer's disease, epilepsy, stress, and depression [5,6]. Therefore, accurate monitoring of these important biomarkers in serum, blood, and urine is very important in early diagnostics [7].

To address this issue, several analytical methods have been developed for in vitro CA monitoring, such as high-performance liquid chromatography (HPLC) [8], HPLC with tandem mass spectrometric detection [9–11], fluorescence [12], and field-effect transistor [13] methods. These methods show high sensitivity and selectivity but require sophisticated and expensive equipment, time-consuming procedures, and skilled operators. Electrochemical methods represent an interesting alternative thanks to their unique advantages, such as their low cost, rapid response, simple operation, and capability for in situ detection [14–17].

Unlike glucose, CAs are redox-active compounds that are easily oxidized in a potential window between 0 and 0.4 V vs. Ag/AgCl [18], depending on the electrode modification. Therefore, total CA concentration can effectively be measured without the use of redox mediators and/or enzymes. The direct oxidation of DA, EP, and NEP on different electrode platforms allowed for the development of several sensors for CA detection [19–25]. However, these sensors suffer from relatively high oxidation potential and electrode surface passivation values due to the electrogenerated phenoxy radicals [26,27]. To this end, attempts at the bio-catalytic oxidation of CA, in particular DA and NEP, have been realized by integrating the Tyr enzyme with conductive nanomaterials and/or polymers on the electrode surface [28,29], leading to significant increases in DA and NEP oxidation peaks with concomitant cathodic shifts in their peak potential. Nevertheless, signal interference from other biological molecules, such as ascorbic acid (AA) and uric acid (UA), which show similar oxidation potentials with overlapping voltametric signals, represents another critical issue for CA detection based on oxidation signals that may limit its applicability. To address this issue, Tyr-based biosensors for CA detection are mainly used by monitoring the reduction signal of the bio-catalytically produced quinone compounds at a relatively moderate potential (about 0.1 V vs. Ag/AgCl on a carbon electrode) [30–32], where no electrochemical interference signal is present. Nanoparticles and/or nanostructures have been integrated into different sensing platforms to enhance both biosensor sensitivity and biosensor selectivity toward CA detection [32–40].

Tyrosinase (Tyr, polyphenol oxidase, EC 1.14.18.1) is a binuclear blue copper protein that acts as a polyphenol oxidase [41]. It catalyzes two consecutive oxidation reactions in presence of molecular oxygen, showing both monophenolase and diphenolase activity: (i) the o-hydroxylation of phenols to guaiacol; and (ii) the oxidation of guaiacol to o-quinones. The biosensor principle is the measurement of the increase in the cathodic signal due to the electrochemical reduction of the o-catecholamine quinone involving two electrons and two protons (Reaction 2), enzymatically generated on the electrode surface by Tyr (Reaction 1), according to the following reactions:

$$\text{Tyr catecholamine} + {}^{1}/_{2}\,O_2 \rightarrow \text{o-catecholamine-quinone} + H_2O \quad (1)$$

$$\text{o-catecholamine-quinone} + 2H^+ + 2e^- \rightarrow \text{catecholamine} + H_2O \quad (2)$$

The signal amplification is assured by the recycling of the o-catecholamine quinone by Tyr enzyme, leading to an enhancement of the selectivity and sensitivity of the biosensor. Therefore, the key factor in biosensor construction is adequate and effective Tyr immobilization in order to enhance the catalytic activity. Common approaches utilized for Tyr immobilization include carbon paste immobilization [42], sol–gel immobilization [43], entrapment within electropolymerized conducting polymers [37], and physical adsorption [44]. A considerable amount of attention has been paid to the use of chitosan (Chit), a polysaccharidic biopolymer composed of glucosamine with proper surface functional groups for biological/chemical binding and/or rapid adsorption [45,46]. It has found a great deal of applicability in sensing applications because of its non-toxicity, biocompatibility, biodegradability, and low cost [45]. Thanks to its polycationic character, chitosan can lock negatively charged proteins by charge attractions and hydrogen-bond interactions. Moreover, the presence of reactive amino and hydroxyl groups in its linear structure allows for covalent protein immobilization through the coupling chemistry via glutaraldehyde or EDC/NHS cross-linking agents [47,48]. However, its poor electrical conductivity may

limit its applicability. To overcome this issue, chitosan has generally been combined with nanomaterials, such as graphene [49], multi-walled carbon nanotubes [50], and metallic nanoparticles [20,34,36], as well as conducting polymers, such as polyaniline and polypyrrole [51,52]. Chitosan nanoparticles (ChitNPs) with a size smaller than 100 nm showed superior chemical and biological performances than pristine chitosan, making them an excellent source for biomedical and biotechnological applications [53,54]. Thanks to their high surface–volume ratio, they can be utilized in biosensing applications as enzyme immobilization supports to achieve ultrasensitive detection of biomolecules. To date, only a few reports have been published with this aim. Anusha et al. [55] immobilized glucose oxidase (GOx) over ChitNPs on a gold electrode and, subsequently, Kim et al. [56] developed a platform based on a poly-γ-glutamic acid/ChitNPs hydrogel, which embedded GOx and magnetic nanoparticles.

In this paper, we report a new biosensing platform for the effective detection of total catecholamine based on the immobilization of Tyr in ChitNPs by using the zero-length EDC-NHS cross-linker on a graphene screen-printed electrode. To the best of our knowledge, no reports are present in the literature on electrode platforms based on a ChitNPs/EDC-NHS/Tyr nanocomposite for CA detection.

2. Experimental

2.1. Chemicals and Reagents

Tyrosinase (EC 1.14.18.1, 8503 U mg^{-1} from mushroom, Tyr), dopamine hydrochloride (DA), epinephrine (EP), norepinephrine (NEP), chitosan (low molecular weight) (Chit), sodium tripolyphosphate (TPP), 1-ethyl-3-(3-dimethylaminopropyl) carbodiimide (EDC), N-hydroxysuccinimide (NHS), ascorbic acid (AA), and uric acid (UA) were purchased from Sigma-Aldrich (St. Louis, MO, USA). Phosphate buffer was prepared with Na_2HPO_4 and NaH_2PO_4. NaOH and HCl were used to adjust pH values. Graphene screen-printed carbon electrodes (GPH/SPEs), used for biosensor construction, were purchased from Dropsens (Metrohm Dropsense, Asturias, Spain, model DRP-110GPH, screen-printed carbon electrodes modified with graphene).

2.2. Apparatus

Electrochemical measurements were performed in a 10 mL conventional three-electrode thermostated glass cell (model 6.1415.150, Metrohm, Herisau, Switzerland) using a graphene screen-printed carbon electrode (GPH/SPE) as a working electrode, an external Ag/AgCl/KCl_{sat} electrode (198 mV vs. NHE) as a reference electrode (cat. 6.0726.100, Metrohm, Herisau, Switzerland), and a glassy carbon rod as a counter electrode (cat. 6.1248.040, Metrohm, Herisau, Switzerland). An Autolab Potentiostat/Galvanostat (Eco Chemie, The Netherlands) was utilized in the electrochemical measurements. Scanning electron microscopy (SEM) and energy-dispersive X-ray spectroscopy (EDX) measurements were performed with a High-Resolution Field Emission Scanning Electron Microscope (HR FESEM, Zeiss Auriga Microscopy, Jena, Germany). The chronoamperometry experiments were carried out using a Sensit/SMART portable potentiostat (PalmSens, Houten, The Netherlands), a smartphone-based sensing device directly connected to a smartphone for POC signal reading.

2.3. Synthesis of Chitosan Nanoparticles

Chitosan nanoparticles (ChitNPs) were synthesized according to an ionic gelation process by adding 9 mL of chitosan dispersion (1 mg mL^{-1}) to 3 mL of TPP solution (1 mg mL^{-1}) and stirring the solution for 2 h at 25 °C with gentle magnetic stirring until an opalescent solution formed. The solution was successively centrifuged for 15 min at 6000 rpm, and the precipitated pellets were rinsed with DI water, dried, and used for further characterization [57].

2.4. Fabrication of TYR/ChitNPs-Modified Electrodes

Two different approaches were employed to immobilize Tyr and ChitNPs on a graphene SPE (the layer-by-layer (LbL) method and the nanoprecipitation (Np) method).

2.4.1. Layer-by-Layer Method

The layer-by-layer method (LbL) consists of the direct deposition "layer-by-layer" of each component of the electrochemical platform (ChitNPs and Tyr) onto the electrode. LbL-Tyr/ChitNPs/GPH/SPE was prepared as follows:

(1) A total of 6 µL of ChitNPs solution (1 mg mL^{-1} in a water solution) was drop-cast onto GPH/SPE and left to dry at room temperature in air for approximately 1 h;
(2) A total of 6 µL of Tyr solution (0.5 mg mL^{-1} in PBS 0.1 M, pH 7.2, KCl 0.1 M) was drop-cast onto the GPH/SPE previously modified with ChitNPs and left to dry at room temperature in air for approximately 1 h.

In the case of LbL-Tyr/EDC-NHS/ChitNPs/GPH/SPE, an additional electrode modification step was introduced between Step 1 and Step 2 by drop-casting onto the electrode surface a mixture of 3 µL of EDC solution (0.5 mM in PBS 0.1 M, pH 7.2, KCl 0.1 M) and 3 µL of NHS solution (0.1 mM in PBS 0.1 M, pH 7.2, KCl 0.1 M).

Three electrodes of each type were prepared in order to evaluate the reproducibility of the biosensor.

2.4.2. Nanoprecipitation Method

In the nanoprecipitation method (Np), Tyr and ChitNPs are co-precipitated in the same solution. Briefly, a solution of ChitNPs (1 mg mL^{-1}) was added to a solution of Tyr (0.5 mg mL^{-1}) under gentle magnetic stirring for 2 h at room temperature and subsequently deposited onto the electrode surface. The Np-Tyr/ChitNPs/GPH/SPE was prepared by drop-casting 12 µL of the Tyr–ChitNPs solution onto the GPH/SPE, which was then dried at room temperature in air for approximately 1 h.

Three Np-Tyr/ChitNPs/GPH/SPEs were prepared in order to evaluate the reproducibility of the biosensor.

2.5. Electrochemical Measurements

Cyclic voltammetry (CV) experiments were performed in PBS at a scan rate of 10 mV s^{-1}. Magnetically stirred PBS (0.1 M, pH 7.2, KCl 0.1 M) was used to perform amperometric measurements. Electrochemical impedance spectroscopy (EIS) was performed at the open circuit potential (OCP) without bias voltage in the 0.1–10^4 Hz frequency range using an ac signal with an amplitude of 10 mV. Differential pulse voltammetry (DPV) experiments were recorded from −0.6 to 0.6 V with an amplitude 20 mV and a step potential of −5 mV. Baseline corrections were done for all DPV data using the NOVA software.

2.6. Preparation of Human Urine Samples

Human urine samples were diluted 100-fold with PBS (0.1 M, pH 7.2; KCl 0.1 M) before all measurements.

3. Results and Discussion

3.1. Characterization of ChitNPs

The morphological analysis of ChitNPs was realized by field emission scanning electron microscopy (FE-SEM) and energy-dispersive X-ray spectroscopy (EDX). Figure 1 shows the FE-SEM images of a bare GPH/SPE before (Panel A) and after (Panel C) the modification with ChitNPs. The bare GPH/SPE showed a densely packed rough surface, consistent with previous literature [58]. The EDX spectrum confirmed the presence of only carbon and oxygen, with an atomic percentage, calculated from the quantification of the peaks, of about 98% and 2%, respectively (Figure 1, Panel B). The FE-SEM image of ChitNPs/GPH/SPE shows aggregates of spherical nanoparticles with different diameters

ranging from 70 to 300 nm (Figure 1, Panel C). The presence of the ChitNP aggregates may be ascribed to the inter- and intra-molecular cross-linkages mediated by the interaction of the positively charged amino groups of Chit and the negatively charged TPP ions [59]. The EDX spectrum of ChitNPs/GPH/SPE (Figure 1, Panel D) confirmed the presence of C (96%), O (3%), and a lower amount of Na (0.5%), probably due to the use of the TPP cross-linker in the procedure for the synthesis of ChitNPs.

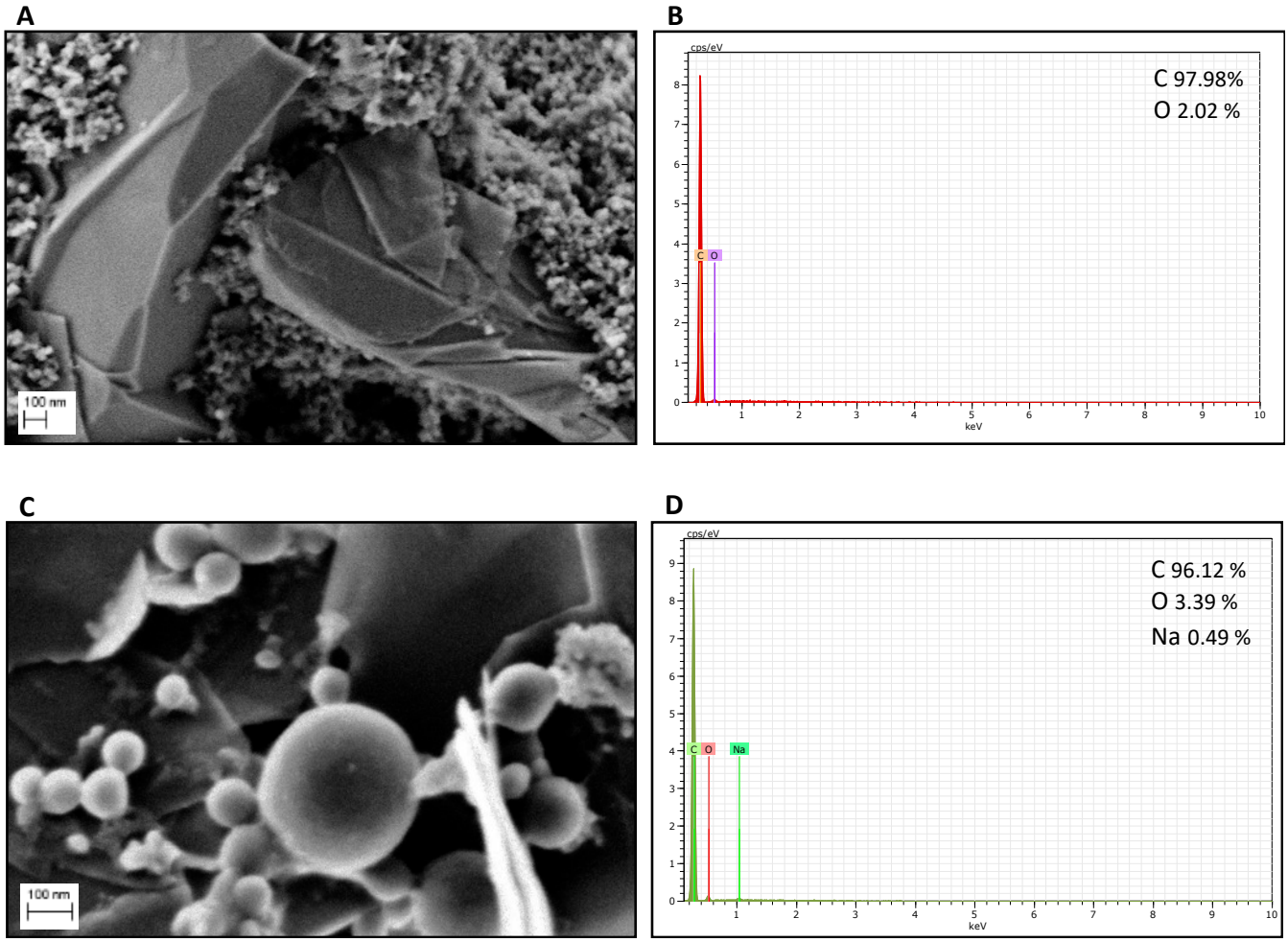

Figure 1. FE-SEM images and EDX spectra for GPH/SPE (Panel (**A**,**B**)) and ChitNPs/GPH/SPE (Panel (**C**,**D**)). Experimental conditions: magnification, 20,000×; voltage, 1.50 kV.

All GPH/SPEs and ChitNPs/GPH/SPEs were subsequently characterized by cyclic voltammetry (CV) experiments in a solution of $Fe(CN)_6^{4-}$ (data not shown) in order to calculate the electroactive area (A_{EA}), the heterogeneous electron transfer rate constant (K_0, cm s^{-1}), and the roughness factor (electroactive–geometrical area ratio, ρ), which are reported in Table S1. The A_{EA} was evaluated using the Randles–Sevick equation by the slope of the peak current vs. the square root of the scan rate ($v^{1/2}$) [60]. The K_0 was calculated using the extended method, which merges the Klingler–Kochi and Nicholson–Shain methods for totally irreversible and reversible systems, respectively [61,62].

3.2. Electrochemical Characterization of the Tyr/ChitNPs Biosensor Platform

The electrochemical characterization of the Tyr/ChitNPs platform was performed using cyclic voltammetry (CV) and electrochemical impedance spectroscopy (EIS).

3.2.1. Optimization of Methods for Loading Tyr on ChitNPs

Two different methods for loading Tyr on the ChitNPs/GHP/SPE platform were investigated by CV experiments: (i) the nanoprecipitation method (Np); and (ii) the layer-by-layer (LbL) method. Figure 2 shows the cyclic voltammograms of DA in the absence (ChitNPs/GPH/SPE, black line) and the presence of Tyr enzyme immobilized by the Np method (Np-Tyr/ChitNPs/GPH/SPE, red line), and the LbL method (LbL-Tyr/ChitNPs/GPH/SPE, blue line) in comparison with Tyr enzyme immobilized on a simple layer of unstructured chitosan (Tyr/Chit/GPH/SPE, green line) deposited by a drop-casting method. Two well-defined redox peaks, due to the oxidation/reduction of DA, are clearly visible on the bare electrode (black curve) without Tyr, while no redox peaks are present with the Tyr/Chit/GPH/SPE electrode (green curve), attesting to the lower conductivity of the unstructured chitosan layer [45] compared with nanostructured chitosan. A similar result was obtained by recording the CVs of DA on a chitosan-modified electrode in the absence of Tyr enzyme (Chit/GPH/SPE). The cyclic voltammogram of DA on ChitNPs/GPH/SPE shows two clear redox peaks (Figure S1, black curve), while smaller oxidation and reduction peaks in the reverse scan can be observed with unstructured chitosan (Figure S1, red curve), thus confirming that the nanostructuration strongly improves the chitosan's conductivity. Similar behavior was described by Marroquin et al. [63], who reported that chitosan nanocomposite films realized with Fe_3O_4 and MWCNTs could simultaneously have enhanced the mechanical properties, thermal stability, and electrical conductivity.

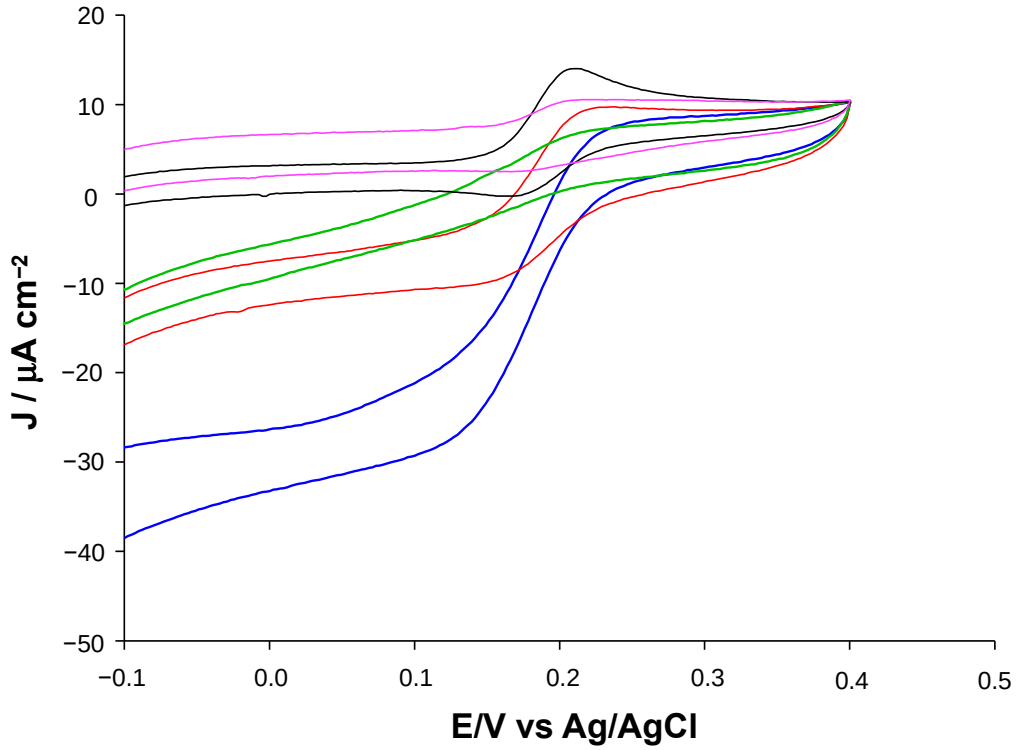

Figure 2. CVs of 50 µM dopamine in PBS (0.1 M, pH 7.2, KCl 0.1 M) on a GPH/SPE (pink line), a ChitNPs/GPH/SPE (black line), a Tyr/Chit/GPH/SPE (green line), a Np-Tyr/ChitNPs/GPH/SPE (red line), and a LbL-Tyr/ChitNPs/GPH/SPE (blue line). Scan rate: 10 mV s^{-1}.

An increase in the reduction peaks was observed for both Np-Tyr/ChitNPs/GPH/SPE (Figure 2, red curve) and LbL-Tyr/ChitNPs/GPH/SPE (Figure 2, blue curve) due to the reduction in the dopamine-o-quinone produced by the enzymatic reaction on the electrode surface to DA [39], demonstrating that the immobilization of Tyr within the nano-biopolymer greatly enhanced the catalytic activity of the enzyme. The reduction peak current of DA on LbL-Tyr/ChitNPs/GPH/SPE was about three times higher than that on Np-Tyr/ChitNPs/GPH/SPE, indicating the superior electrochemical perfor-

mances of the LbL loading method in terms of the better electron transfer between the dopamine-o-quinone and the electrode surface [64]. The results reveal that the LbL immobilization method promotes the Tyr's catalytic property better than the Np method and probably plays a significant role in: (i) the improvement of enzyme immobilization by favoring physical adsorption and the formation of electrostatic interactions between positively charged ChitNPs [57] and negatively charged Tyr enzyme [41]; and (ii) facilitating the direct electron transfer between the substrate molecules and the modified electrode surface.

3.2.2. Optimization of Tyr Concentration

The amount of immobilized enzyme is one of the most relevant parameters in electrode modification. Figure 3 shows the effect of the concentration of Tyr, immobilized by the LbL method on the Tyr/ChitNPs/GPH/SPE, on the cathodic peak current registered in the presence of 50 μM DA. The intensity current differences (ΔI), calculated as the current differences obtained in the presence and the absence of Tyr, increase with decreasing concentrations of Tyr immobilized on the electrode surface. The optimal Tyr concentration was found to be 0.5 mg mL^{-1}, attesting to the fact that electron transfer might be hindered at higher enzyme concentrations. Lower concentrations were also tested, showing no significant increase in the ΔI values.

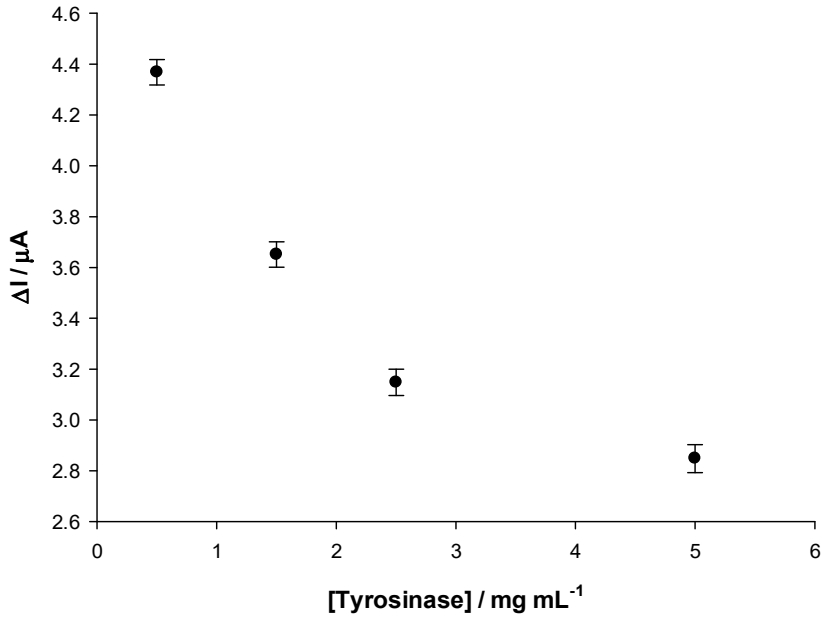

Figure 3. Effect of Tyr concentration on the cathodic peak current of the Tyr/ChitNPs/GPH/SPE in PBS (0.1 M, pH 7.2, KCl 0.1 M) with 50 μM DA.

3.2.3. Tyrosinase Covalent Functionalization via EDC-NHS Coupling Chemistry

In order to enhance the efficacy of the Tyr-based biosensor, the Tyr covalent immobilization strategy using EDC-NHS as a cross-linking agent was investigated. The EDC-NHS coupling chemistry takes advantage of the properties of the EDC-NHS cross-linker, which is able to form amide bonds between carboxyl and amine groups, as shown in Scheme 1 [48]. In particular, the carboxyl groups of ChitNPs immobilized on the electrode surface are activated by the EDC/NHS, forming a typical NHS-ester, and, subsequently, the amino group from the Tyr enzyme acts on this NHS-ester, forming a very strong covalent amidic linkage.

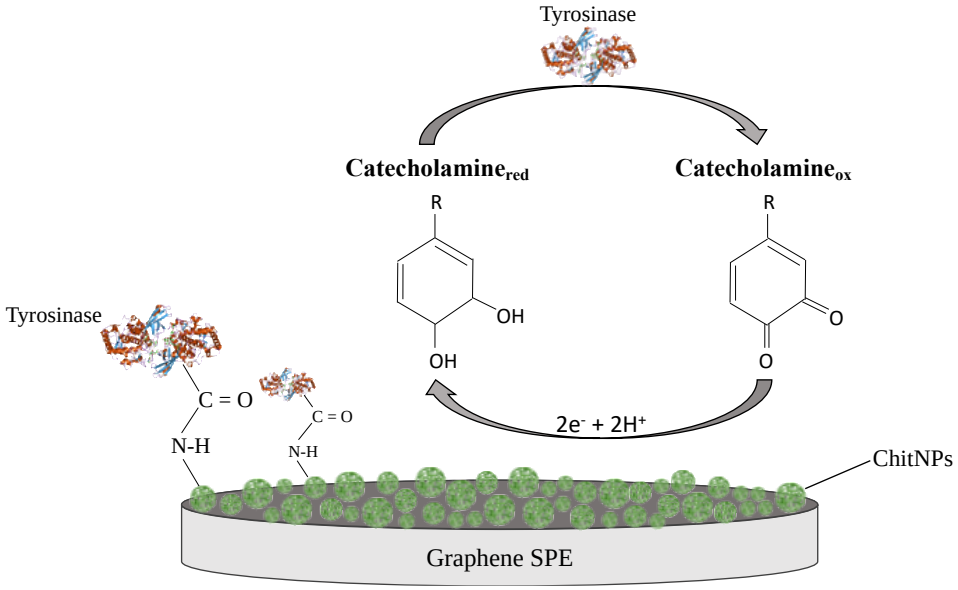

Scheme 1. Schematic representation of the Tyr/EDC-NHS/ChitNPs/GPH-SPE electrochemical platform and the CA biosensor mechanism.

Figure 4 shows the cyclic voltammograms of DA in pH 7.2 PBS on ChitNPs/GPH/SPE (black line) and LbL-Tyr/ChitNPs/GPH/SPE without (blue line) and with (red line) the EDC-NHS cross-linking agent. The reduction peak current of DA observed on LbL-Tyr/EDC-NHS/ChitNPs/GPH/SPE was 1.5 times higher than that on LbL-Tyr/ChitNPs/GPH/SPE, attesting to the enhanced electrochemical performances of the method based on covalent functionalization compared with the LbL method utilizing simple electrostatic interactions, probably thanks to the higher stability of the covalently immobilized Tyr for enhanced biocatalysis.

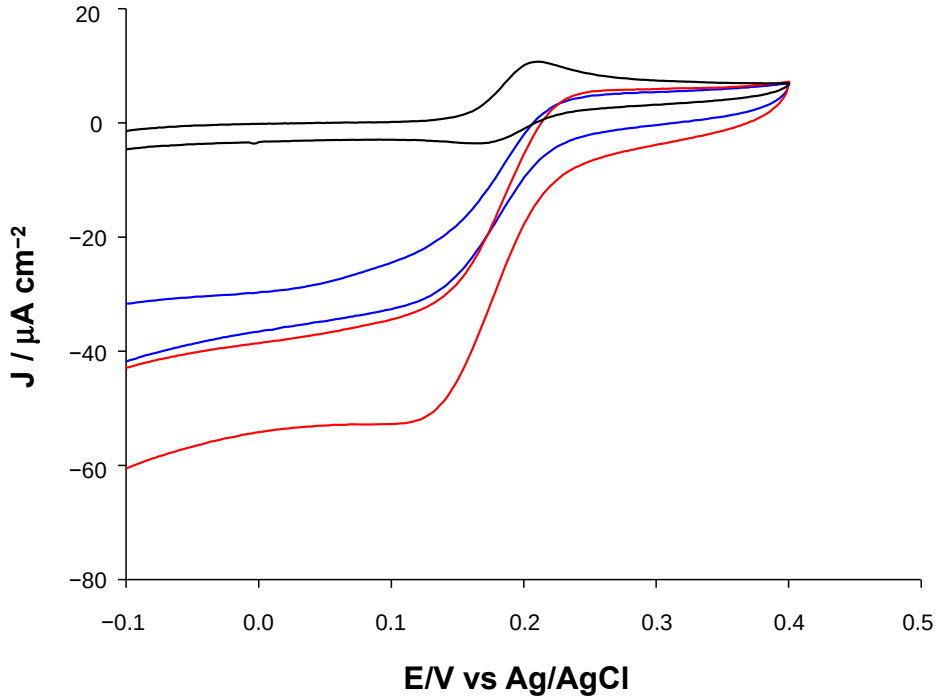

Figure 4. CVs of 50 µM DA in PBS (0.1 M, pH 7.2, KCl 0.1 M) on a ChitNPs/GPH/SPE (black line), a LbL-Tyr (0.5 mg/mL)/ChitNPs/GPH/SPE (blue line), and a LbL-Tyr (0.5 mg/mL)/EDC-NHS/ChitNPs/GPH/SPE (red line). Scan rate: 10 mV s^{-1}.

3.2.4. Electrochemical Impedance Spectroscopy Behavior of the Modified Electrodes

The EIS technique was used to investigate the electrochemical properties of the modified electrodes after each surface modification step. Figure 5 shows the Nyquist plots of the ChitNPs/GPH/SPE (black), the Tyr/ChitNPs/GPH/SPE (blue), and the Tyr/EDC-NHS/ChitNPs/GPH/SPE (red) in 5 mM $[Fe(CN)_6]^{3-/4-}$ solution. The semicircle diameter of the Nyquist plot represents the charge transfer resistance (Rct), which is related to small changes at the electrode–electrolyte interface in the solution. The immobilization of a protein biomolecule over the electrode surface causes an increase in the Rct value that is related to the hindering of the electron transfer between the redox probe and the electrode surface. The impedance spectra were fitted by using the simple Randles circuit (R(Q(RW))) reported in Figure 5. Experimental R_{ct} values are in the following order: ChitNPs/GPH/SPE (357 Ω) < Tyr/ChitNPs/GPH/SPE (403 Ω) < Tyr/EDC-NHS/ChitNPs/GPH/SPE (436 Ω) due to the hampering effect of Tyr on the charge transfer. The Rct values confirm the successful immobilization of Tyr enzyme on the electrode surface, resulting in strong optimization with the use of the EDC-NHS cross-linker (red curve).

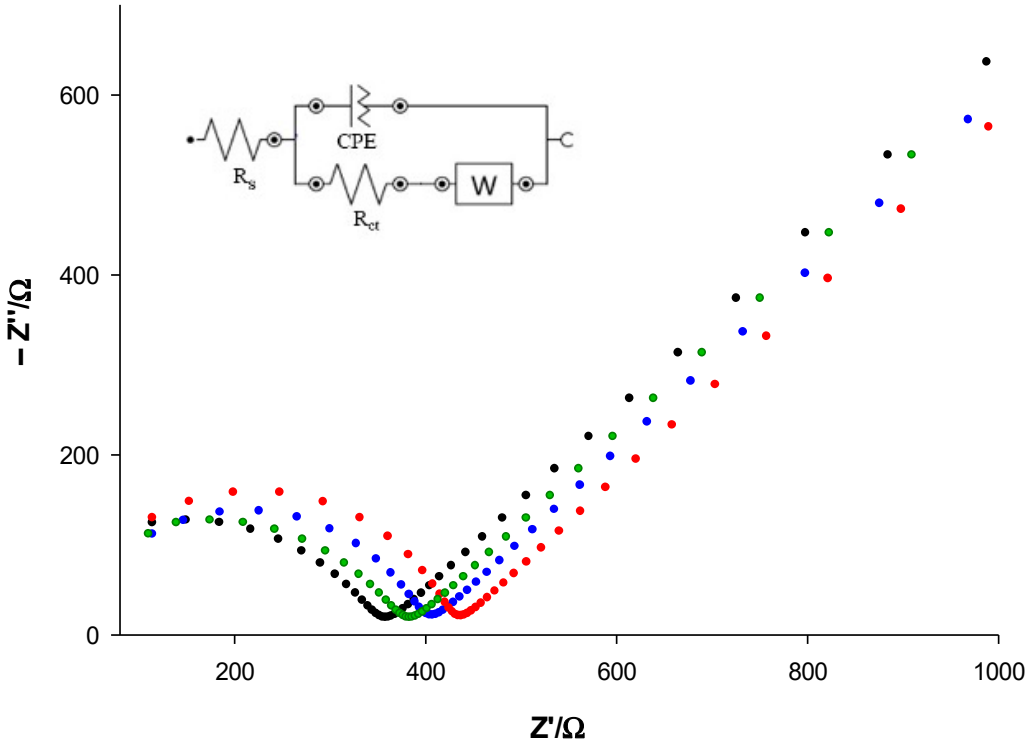

Figure 5. Nyquist plots of GPH/SPE (green), ChitNPs/GPH/SPE (black), Tyr/ChitNPs/GPH/SPE (blue), and Tyr/EDC-NHS/ChitNPs/GPH/SPE (red) measured in the presence of 5 mM $[Fe(CN)_6]^{3-/4-}$ containing 0.1 M KCl solution. The inset shows the equivalent circuit used for fitting the experimental data.

3.3. Amperometric Response of Dopamine

Figure 6 (Panel A and B) illustrates a typical steady-state current–time response upon successive additions of DA on Tyr/ChitNPs/GPH/SPE (Panel A) and Tyr/EDC-NHS/ChitNPs/GPH/SPE (Panel B), showing a fast response time (3 s). The measurements were carried out by immersing the modified electrode in blank PBS (0.1 M). Once a steady baseline was achieved, DA was added to the solution, causing an increase in the cathodic current due to the reduction in o-quinone generated by the enzymatic oxidation of DA [64]. Thus, the target DA molecule was regenerated during the reduction reaction at the electrode, allowing for the amplification of the electrochemical signal, which leads to enhanced sensitivity [65]. Figure 6 (Panel C) exhibits the typical calibration curves of the DA biosensors corresponding to the electrode platforms with (black curve) and without

(red curve) EDC-NHS, both following Michelis–Menten kinetics. As can be seen in the inset of Panel C, the linear range spanned from 4 μM to 12 μM with a regression equation of $y = 0.03325x + 0.0404$ ($R^2 = 0.994$) and from 0.5 μM to 5 μM with a regression equation of $y = 0.80066x + 0.0039121$ ($R^2 = 0.997$) in the case of the Tyr/ChitNPs/GPH/SPE biosensor and the Tyr/EDC-NHS/ChitNPs/GPH/SPE biosensor, respectively. The biosensor based on the EDC-NHS cross-linker showed a lower LOD of 0.17 μM and a two-fold higher sensitivity of 0.583 μA mM^{-1} cm^{-2} compared with the corresponding biosensor without EDC-NHS. According to the Lineweaver–Burk equation [66], the apparent Michaelis–Menten constants (K_M^{app}) were 25.59 and 9.51 μM for the Tyr/ChitNPs/GPH/SPE biosensor and the Tyr/EDC-NHS/ChitNPs/GPH/SPE biosensor, respectively. It is interesting to note that the experimental K_M^{app} value is lower than the K_M value of the free enzyme towards dopamine (K_M = 2.2 mM) [67], attesting to the optimal accessibility of the target molecules to the active sites of the enzyme. The electrochemical characteristics of the two biosensors in terms of the K_M^{app}, maximum current density, linearity range, LOD, and sensitivity are summarized in Table 1.

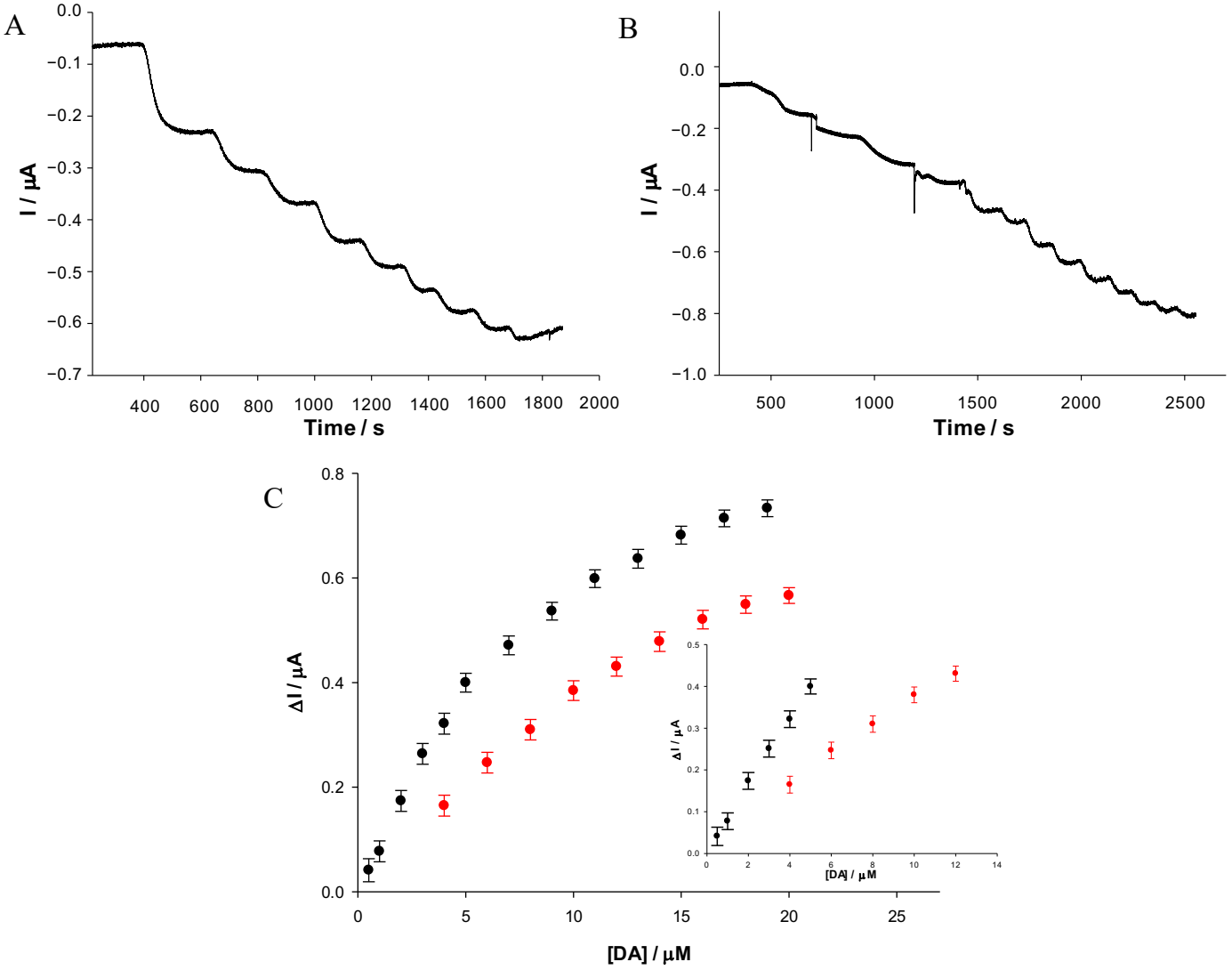

Figure 6. Typical chronoamperometric curves of Tyr/ChitNPs/GPH/SPE (Panel **A**) and Tyr/EDC-NHS/ChitNPs/GPH/SPE (Panel **B**) upon successive additions of different concentrations of DA to the stirred PBS (0.1 M, pH 7.2, KCl 0.1 M) (applied potential: 0 V vs. Ag/AgCl) and the relative calibration curves of Tyr/ChitNPs/GPH/SPE (Panel **C**, red curve) and Tyr/EDC-NHS/ChitNPs/GPH/SPE (Panel **C**, black curve) as a function of DA concentration. Inset: the magnification of the linear range.

Table 1. Comparison of the kinetic and analytical characteristics of DA biosensors with different electrochemical platforms.

Modified SPE	K_M^{app} (μM)	J_{max} (μA cm^{-2})	Linear Range (μM)	LOD (μM)	Sensitivity (μA μM^{-1} cm^{-2})	R^2
Tyr/ChitNPs/GPH	25.59 ± 3.013	11.1 ± 0.84	4–12	1.36	0.275	0.994
Tyr/EDC-NHS/ChitNPs/GPH	9.51 ± 0.544	9.16 ± 0.009	0.5–5	0.17	0.583	0.996

3.4. Amperometric Response of Epinephrine and Norepinephrine

The Tyr/EDC-NHS/ChitNPs/GPH/SPE-based biosensor, which showed the best performance, was utilized for EP and NEP detection. Chronoamperometric experiments were performed at an applied potential of 0 V vs. Ag/AgCl as EP and NEP gave cathodic peaks at the same redox potential of DA (curves not shown). The corresponding calibration plots are reported in Figure 7, together with the calibration plot of DA (black curve) as a comparison. Table 2 summarizes the analytical and kinetic performances of the proposed biosensor for the three catecholamines studied, including the linear range, LOD, sensitivity, maximum current density, and K_M^{app}. The sensitivity of the DA biosensor was 5 times higher than that of EP and NEP. The K_M^{app} values were in the following order: DA < NEP < EP, attesting to the stronger affinity and binding of the Tyr enzyme to DA, leading to a higher catalytic activity [27].

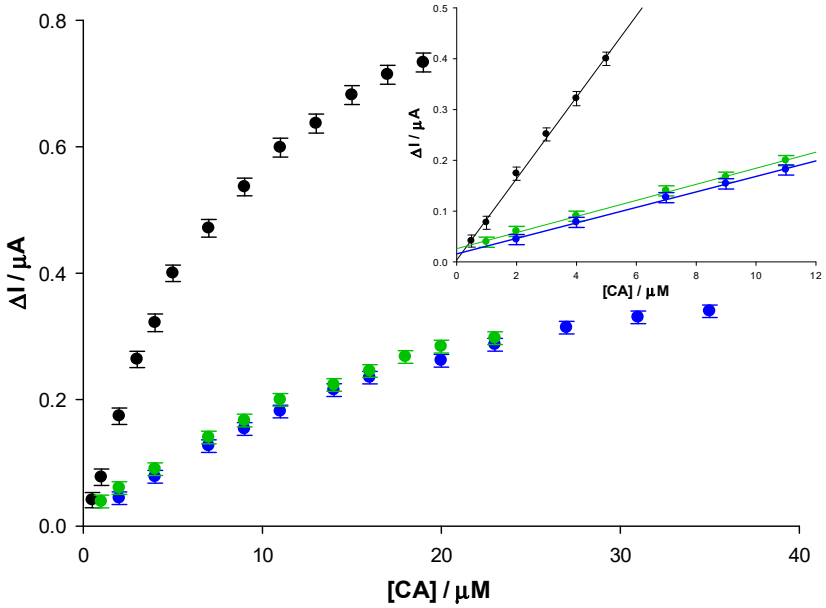

Figure 7. Calibration curves of Tyr/EDC-NHS/ChitNPs/GPH/SPE as a function of the concentration of catecholamine: DA (black curve), EP (blue curve), and NEP (green curve). Inset: the magnification of the linear range.

Table 2. Comparison of the kinetic and analytical characteristics of Tyr/EDC-NHS/ChitNPs/GPH/SPE biosensors with different catecholamines.

Catecholamine	K_M^{app} (μM)	J_{max} (μA cm^{-2})	Linear Range (μM)	LOD (μM)	Sensitivity (μA μM^{-1} cm^{-2})	R^2
DA	9.51 ± 0.544	9.16 ± 0.009	0.5–5	0.17	0.583	0.996
EP	25.46 ± 1.095	4.95 ± 0.099	2–11	0.71	0.125	0.998
NEP	20.83 ± 2.2807	4.74 ± 0.323	1–11	0.40	0.132	0.995

The total catecholamine concentration is therefore expressed as a DA concentration, thanks to the best analytical and kinetic performance of this biosensor.

Table 3 shows a comparison between the results obtained with our biosensor and other Tyr-based biosensors for catechol and catecholamine recently reported in the literature.

It is possible to observe that the proposed ChitNPs/graphene platform shows superior analytical performances compared with the other platforms for CA detection, whereas inferior performances can be observed when compared with Tyr-based catechol biosensors. These results can be ascribed to the stronger affinity of the Tyr enzyme to catechol.

Table 3. Comparison of Tyr-based biosensors reported in the literature.

Catecholamine/Catechol	Biosensor Platform	Linear Range (μM)	LOD (μM)	Ref.
catechol	Tyr/BOND/film electrode	5–120	2.35	[68]
DA	Tyr/MWNT/GCE	50–1000	50	[69]
catechol	PPy-NTs/PPO	0.1–35	0.0012	[70]
catechol	PEDOT-rGO-Fe_2O_3-PPO	0.04–62	0.007	[71]
catechol	Tyr-AuNPs-DHP/GCE	2.5–95	0.17	[72]
catechol	Tyr-PAMAM-Sil-rGO/GCE	0.01–22	0.006	[73]
catechol	Tyr/PAMAM/GO-CMC/GCE	0.002–0.4	0.0009	[74]
catechol	Tyr/GO/GA/GCE	0.05–50	0.03	[31]
NEP	Tyr-CDs-CA/Au-E	1–200	0.196	[29]
DA	Tyr-CoP-Au	2–30	0.43	[27]
DA	IDE/PEDOT-CNT-Tyr-GAD-HFR	100–500	11	[75]
DA	Tyr-SWNTs-Ppy	5–50	5	[76]
EP	Tyr/TBT-film/Au	0.1–50	0.06	[77]
DA	Tyr/EDC-NHS/ChitNPs/GPH	0.5–5	0.17	this work

3.5. Selectivity

The selectivity of the Tyr/EDC-NHS/ChitNPs/GPH/SPE-based biosensor for DA was investigated by recording the current response in the presence of potential interferents, which can coexist in biological matrices. In particular, differential pulse voltammograms were recorded in a solution containing a 100-fold concentration of ascorbic acid (AA) and uric acid (UA) in the presence of DA. AA and UA usually show overlapping voltametric curves on both unmodified and chemically modified electrodes [23]. As shown in Figure 8, three well-resolved cathodic peaks were recorded at about −450, +100, and +400 mV for AA, DA, and UA, respectively. The results clearly demonstrate that AA and UA did not significantly interfere with DA detection, showing the high selectivity of the proposed biosensor.

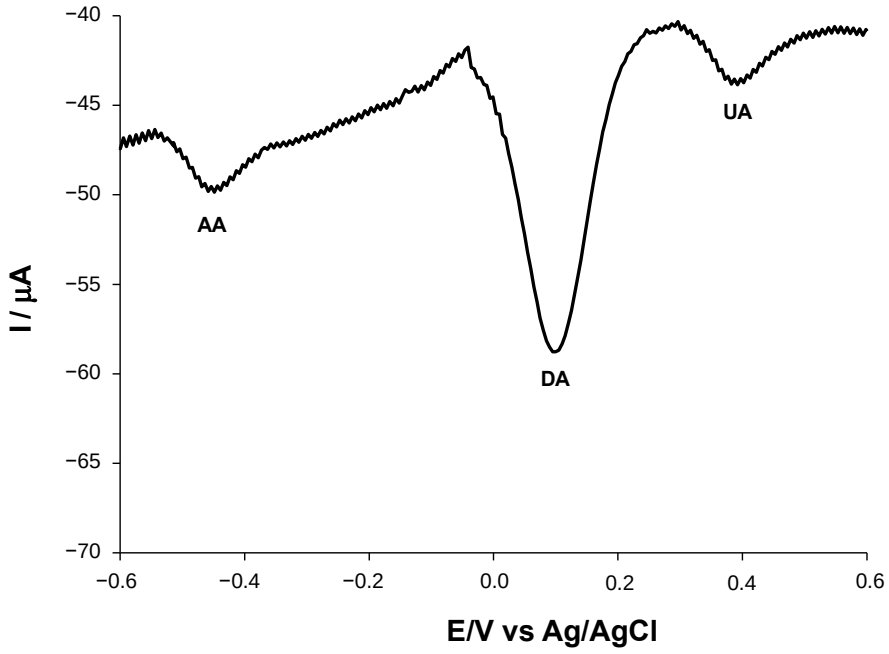

Figure 8. DPVs of 20 μM DA in the presence of 2 mM AA and 2 mM UA with the Tyr/EDC-NHS/ChitNPs/GPH/SPE biosensor.

3.6. Stability

The stability and lifetime of the biosensor for DA, EP, and NEP detection were investigated by measuring the DPV responses of the biosensor every 5 days (10 measurements) over a period of 30 days using a 10 μM solution of each CA (Figure S2). The biosensor was stored in a dry refrigerator at 4 °C in between the measurements. The stability was good as the biosensor retained about 90% of its initial current response after 30 days. These results may be ascribed to the synergistic effect of the bio-nanocomposite including ChitNPs and graphene, which reduces the enzyme denaturation and the subsequent loss of catalytic properties.

3.7. Real Sample Detection

Finally, the Tyr/EDC-NHS/ChitNPs/GPH/SPE-based biosensor was tested in human urine samples spiked with known concentrations of DA in order to evaluate the effectiveness of the biosensor in physiological samples. A fixed amount of DA (5 μM) was added to three urine samples without any sample pretreatment. All measurements were done in triplicate using chronoamperometry and the results are reported in Table 4. The recovery rates ranged from 94% to 98% and the relative standard deviation (RSD) values did not exceed 6.3%, demonstrating the efficacy of the proposed biosensor in real samples.

Table 4. Determination of DA in urine samples (n = 3) using the calibration curve from Figure 6.

Sample	Added (μM)	Found (μM)	Recovery (%)	RSD (n = 3) (%)	Spectrophotometric Method (μM)
Sample 1	5	4.8	96	4.2	5.10
Sample 2	5	4.9	98	2.1	5.25

The results were subsequently compared to those obtained with a standard spectrophotometric method used as reference (Table 3). An unpaired *t*-test was performed, and the results show that there was no statistically significant difference in the DA quantification between the proposed biosensor and the standard spectrophotometric method ($t = -2429$; degrees of freedom = 4; $p = 0.072$). This result indicates the biosensor's excellent capacity to provide mean values close to those obtained when the same samples are measured by using the standard spectrophotometric method.

4. Conclusions

In this work, we demonstrated the feasibility of developing an amperometric biosensor for total catecholamine detection by using a novel electrochemical nano-platform based on the immobilization of Tyr/ChitNPs on a graphene SPE. The ChitNPs were synthesized by the ionic gelation process and subsequently immobilized with Tyr enzyme on the graphene electrode through a layer-by-layer approach with and without EDC-NHS as a cross-linking agent. The ChitNPs provided a friendly environment for Tyr immobilization, thus enhancing the catalytic activity of the enzyme and, at the same time, showing an improved platform conduction pathway thanks to the higher conductivity compared with pristine chitosan. The ChitNPs/EDC-NHS/graphene nanocomposite matrix showed superior electrochemical performances, which can be attributed to the synergistic effect of graphene and ChitNPs. The excellent conductivity and large surface area of the graphene electrode in combination with the properties of the ChitNPs produced the good analytical performances of the developed catecholamine biosensor in terms of a short response time (3 s), high sensitivity, a low detection limit, good stability, and satisfactory recovery when tested in spiked human urine samples. At the current state of research, the proposed ChitNPs/graphene platform does not provide superior performance compared with other nanostructured platforms for CA detection reported in the literature, but the ease of preparation and low cost of the proposed ChitNPs make them a promising component and/or additive for electrochemical biosensor platforms thanks to the described beneficial properties.

Supplementary Materials: The following supporting information can be downloaded at: https://www.mdpi.com/article/10.3390/bios12070519/s1, Table S1: Electrochemical parameters related to GPH/SPE and ChitNPs/GPH/SPE modiefied electrode: electroactive area (A_{EA}), roughness factor (ρ) and heterogenous electron transfer rate costant (K_0). Experimental condition: 1.1 mM $Fe(CN)_6^{4-}$ in 0.1 M KCl; Figure S1: CVs of 50 µM Dopamine in PBS 0.1 M (pH 7.2; KCl 0.1 M), on a ChitNPs/GPH/SPE (black line) and Chit/GPH/SPE (red line); Figure S2: Stability measurements over a period of 30 days in presence of 10 µM of DA (Panel A), EP (Panel B) and NEP (Panel C) in PBS 0.1 M (pH 7.2; KCl 0.1 M); Figure S3: Optimization of applied potential with Tyr/EDC-NHS/ChitNPs/GPH/SPE in 50 mM dopamine in 0.1 M PBS (pH 7.2; KCl 0.1 M).

Author Contributions: Investigation: V.G., C.T.; Methodology: E.C.; Resources: A.A., A.L.; Supervision: R.A.; Writing original draft: V.G., R.A. All authors have read and agreed to the published version of the manuscript.

Funding: This work was supported by the Italian Ministry of Education, Universities, and Research (Progetto di Ateneo 2022, No. RP12117A8B0CA73F).

Institutional Review Board Statement: Not applicable.

Informed Consent Statement: Not applicable.

Data Availability Statement: Not applicable.

Acknowledgments: The authors would like to thank Andrea Isidori and Mary Anna Venneri of the Department of Experimental Medicine, Sapienza University of Rome, for the support provided.

Conflicts of Interest: The authors declare no conflict of interest.

References

1. Emran, M.Y.; Shenashen, M.A.; Abdelwahab, A.A.; Khalifa, H.; Mekawy, M.; Akhtar, N.; Abdelmottaleb, M.; EI-Safty, S.A.J. Design of hierarchical electrocatalytic mediator for one step, selective screening of biomolecules in biological fluid samples. *Appl. Electrochem.* **2018**, *48*, 529–542. [CrossRef]
2. Li, L.; Lu, Y.Z.; Qian, Z.; Yang, Z.; Yang, K.; Zong, S.; Wang, Z.; Cui, Y. Ultra-sensitive surface enhanced Raman spectroscopy sensor for in-situ monitoring of dopamine release using zipper-like ortho-nanodimers. *Biosens. Bioelectron.* **2021**, *180*, 113100. [CrossRef] [PubMed]
3. Liss, B.; Roeper, J. Individual dopamine midbrain neurons: Functional diversity and flexibility in health and disease. *Brain Res. Rev.* **2008**, *58*, 314–321. [CrossRef] [PubMed]
4. Bucolo, C.; Leggio, G.M.; Drago, F.; Salomone, S. Dopamine outside the brain: The eye, cardiovascular system and endocrine pancreas. *Pharmacol. Ther.* **2019**, *203*, 107392. [CrossRef] [PubMed]
5. Klein, M.O.; Battagello, D.S.; Cardoso, A.R.; Hauser, D.N.; Bittencourt, J.C.; Correa, R.G. Dopamine: Functions, Signaling, and Association with Neurological Diseases. *Cell. Mol. Neurobiol.* **2019**, *39*, 31–59. [CrossRef]
6. Medina, M.Á.; Urdiales, J.L.; Rodríguez-Caso, C.; Ramírez, F.J.; Sánchez-Jiménez, F. Biogenic amines and polyamines: Similar biochemistry for different physiological missions and biomedical applications. *Crit. Rev. Biochem. Mol. Biol.* **2003**, *38*, 23–59. [CrossRef]
7. Marc, D.T.; Ailts, J.W.; Ailts Campeau, D.C.; Bull, M.J.; Olson, K.L. Neurotransmitters excreted in the urine as biomarkers of nervous system activity: Validity and clinical applicability. *Neurosci. Biobehav. Rev.* **2011**, *35*, 635–644. [CrossRef]
8. Carrera, V.; Sabater, E.; Vilanova, E.; Sogorb, M.A. A simple and rapid HPLC–MS method for the simultaneous determination of epinephrine, norepinephrine, dopamine and 5-hydroxy- tryptamine: Application to the secretion of bovine chromaffin cell cultures. *J. Chromatogr. B Anal. Technol. Biomed. Life Sci.* **2007**, *847*, 88–94. [CrossRef]
9. Mizuguchi, H.; Nishimori, D.; Kuwabara, T.; Takeuchi, M.; Iiyama, M.; Takayanagi, T. Track-etched membrane-based dual-electrode coulometric detector for microbore/capillary high-performance liquid chromatography. *Anal. Chim. Acta* **2020**, *1102*, 46–52. [CrossRef]
10. Matuszewski, B.K.; Constanzer, M.L.; Chavez-Eng, C.M. Strategies for the Assessment of Matrix Effect in Quantitative Bioanalytical Methods Based on HPLC-MS/MS. *Anal. Chem.* **2003**, *75*, 3019–3030. [CrossRef]
11. Moghzi, F.; Soleimannejad, J.; Sañudo, E.C.; Janczak, J. Dopamine Sensing Based on Ultrathin Fluorescent Metal–Organic Nanosheets. *ACS Appl. Mater. Interfaces* **2020**, *12*, 44499–44507. [CrossRef] [PubMed]
12. Liu, N.; Xiang, X.; Fu, L.; Cao, Q.; Huang, R.; Liu, H.; Han, G.; Wu, L. Regenerative field effect transistor biosensor for in vivo monitoring of dopamine in fish brains. *Biosens. Bioelectron.* **2021**, *188*, 113340. [CrossRef] [PubMed]
13. Ribeiro, J.A.; Fernandes, P.M.V.; Pereira, C.M.; Silva, F. Electrochemical sensors and biosensors for determination of catecholamine neurotransmitters: A review. *Talanta* **2016**, *160*, 653–679. [CrossRef] [PubMed]

14. Xu, C.; Gu, C.; Xiao, Q.; Chen, J.; Yin, Z.Z.; Liu, H.; Fan, K.; Li, L. A highly selective and sensitive biosensor for dopamine based on a surface molecularly imprinted layer to coordinate nano-interface functionalized acupuncture needle. *Chem. Eng. J.* **2022**, *436*, 135203. [CrossRef]
15. Rahman, S.F.; Min, K.; Park, S.H.; Park, J.H.; Yoo, J.C.; Park, D.H. Selective determination of dopamine with an amperometric biosensor using electrochemically pretreated and activated carbon/tyrosinase/Nafion®-modified glassy carbon electrode. *Biotechnol. Bioprocess Eng.* **2016**, *21*, 627–633. [CrossRef]
16. Rand, E.; Periyakaruppan, A.; Tanaka, Z.; Zhang, D.A.; Marsh, M.P.; Andrews, R.J.; Lee, K.H.; Chen, B.; Meyyappan, M.; Koehne, J.E. A carbon nanofiber-based biosensor for simultaneous detection of dopamine and serotonin in the presence of ascorbic acid. *Biosens. Bioelectron.* **2013**, *42*, 434–438. [CrossRef]
17. De-Qian, H.; Cheng, C.; Yi-Ming, W.; Hong, Z.; Liang-Quan, S.; Hua-Jie, X.; Zhao-Di, L. The Determination of Dopamine Using Glassy Carbon Electrode Pretreated by a Simple Electrochemical Method. *J. Electrochem. Sci.* **2012**, *7*, 5510–5520.
18. Gao, F.; Cai, X.; Wang, X.; Gao, C.; Liu, S.; Gao, F.; Wang, Q. Highly sensitive and selective detection of dopamine in the presence of ascorbic acid at graphene oxide modified electrode. *Sens. Actuators B Chem.* **2013**, *186*, 380–387. [CrossRef]
19. Qiu, H.J.; Zhou, G.P.; Ji, G.L.; Zhang, Y.; Huang, X.R.; Ding, Y. A novel nanoporous gold modified electrode for the selective determination of dopamine in the presence of ascorbic acid. *Coll. Surf. B Biointerfaces* **2008**, *69*, 105–108. [CrossRef]
20. Üge, A.; Zeybek, D.K.; Zeybek, B. An electrochemical sensor for sensitive detection of dopamine based on MWCNTs/CeO_2-PEDOT composite. *J. Electroanal. Chem.* **2018**, *15*, 134–142. [CrossRef]
21. Yang, C.; Jacobs, C.B.; Nguyen, M.D.; Ganesana, M.; Zestos, A.G.; Ivanov, I.N.; Puretzky, A.A.; Rouleau, C.M.; Geohegan, D.B.; Venton, B.J. Carbon nanotubes grown on metal microelectrodes for the detection of dopamine. *Anal. Chem.* **2016**, *88*, 645–652. [CrossRef] [PubMed]
22. Deepika, J.; Sha, R.; Badhulika, S. A ruthenium (IV) disulfide based non-enzymatic sensor for selective and sensitive amperometric determination of dopamine. *Microchim. Acta* **2019**, *186*, 480. [CrossRef] [PubMed]
23. Tortolini, C.; Cass, A.E.G.; Pofi, R.; Lenzi, A.; Antiochia, R. Microneedle-based nanoporous gold electrochemical sensor for real-time catecholamine detection. *Microchim. Acta* **2022**, *189*, 1–14. [CrossRef] [PubMed]
24. Mphuthi, N.G.; Adekunle, A.S.; Ebenso, E.E. Electrocatalytic oxidation of epinephrine and norepinephrine at metal oxide doped phthalocyanine/MWCNT composite sensor. *Sci. Rep.* **2016**, *6*, 26938. [CrossRef]
25. Wang, J.; Martinez, T.; Yaniv, D.R.; McCormick, L.D. Scanning tunneling microscopic investigation of surface fouling of glassy carbon surfaces due to phenol oxidation. *J. Electroanal. Chem. Interfacial Electrochem.* **1991**, *313*, 129–140. [CrossRef]
26. Lane, R.F.; Blaha, C.D. Detection of catecholamines in brain tissue: Surface-modified electrodes enabling in vivo investigations of dopamine function. *Langmuir* **1990**, *6*, 56–65. [CrossRef]
27. Florescu, M.; David, M. Tyrosinase-based biosensors for selective dopamine detection. *Sensors* **2017**, *17*, 1314. [CrossRef]
28. Apetrei, I.M.; Apetrei, C. Development of a novel biosensor based on tyrosinase/platinum nanoparticles/Chitosan/graphene nanostructured layer with applicability in bioanalysis. *Materials* **2019**, *12*, 1009. [CrossRef]
29. Baluta, S.; Lesiak, A.; Cabaj, J. Simple and cost-effective electrochemical method for norepinephrine determination based on carbon dots and tyrosinase. *Sensors* **2020**, *20*, 4567. [CrossRef]
30. Apetrei, I.M.; Apetrei, C. Biosensor based on tyrosinase immobilized on a single-walled carbon nanotube-modified glassy carbon electrode for detection of epinephrine. *Int. J. Nanomed.* **2013**, *8*, 4391–4398. [CrossRef]
31. Wang, Y.; Zhai, F.; Hasebe, Y.; Jia, H.; Zhang, Z. A highly sensitive electrochemical biosensor for phenol derivatives using a graphene oxide-modified tyrosinase electrode. *Bioelectrochem* **2018**, *122*, 174–182. [CrossRef] [PubMed]
32. Janegitz, B.C.; Medeiros, R.A.; Rocha-Fillo, R.C.; Fatibello-Filho, O. Direct electrochemistry of tyrosinase and biosensing for phenol based on gold nanoparticles electrodeposited on a boron-doped diamond electrode. *Diam. Relat. Mater.* **2012**, *25*, 128–133. [CrossRef]
33. Yang, L.; Xiong, H.; Zhang, X.; Wang, S. A novel tyrosinase biosensor based on chitosan-carbon-coated nickel nanocomposite film. *Bioelectrochem* **2012**, *84*, 44–48. [CrossRef] [PubMed]
34. Vicentini, F.C.; Janegitz, B.C.; Brett, C.M.A.; Fatibello-Filho, O. Tyrosinase biosensor based on a glassy carbon electrode modified with multi-walled carbon nanotubes and 1-butyl-3-methylimidazolium chloride within a dihexadecylphosphate film. *Sens. Actuators B Chem.* **2013**, *188*, 1101–1108. [CrossRef]
35. Fartas, F.M.; Abdullah, J.; Yusof, N.A.; Sulamain, Y.; Saiman, M.I. Biosensor based on tyrosinase immobilized on graphene-decorated gold nanoparticle chitosan for phenolic detection in aqueous. *Sensors* **2017**, *17*, 1132. [CrossRef] [PubMed]
36. Apetrei, C.; Rodriguez-Mendez, M.L.; De Saja, J.A. Amperometric tyrosinase based biosensor using an electropolymerized phosphate-doped polypyrrole film as an immobilization support. Application for detection of phenolic compounds. *Electrochim. Acta* **2011**, *56*, 8919–8925. [CrossRef]
37. Wee, Y.; Park, S.; Kwon, Y.H.; Ju, Y.; Yeon, K.M.; Kim, J. Tyrosinase-immobilized CNT based biosensor for highly-sensitive detection of phenolic compounds. *Biosens. Bioelectron.* **2019**, *132*, 279–285. [CrossRef] [PubMed]
38. Da Silva, W.; Ghica, M.E.; Ajayi, R.F.; Iwuoha, E.I.; Brett, C.M.A. Tyrosinase based amperometric biosensor for determination of tyramine in fermented food and beverages with gold nanoparticles doped poly(8-anilino-1-naphtalene sulphonic acid) modified electrode. *Food Chem.* **2019**, *282*, 18–26. [CrossRef]
39. Kim, D.S.; Kang, E.S.; Seungho, B.; Choo, S.S.; Chung, Y.H.; Lee, D.; Min, J.; Kim, T.H. Electrochemical detection of dopamine using periodic cylindrical gold nanoelectrode arrays. *Sci. Rep.* **2018**, *8*, 14049. [CrossRef]

40. Sainio, S.; Palomaki, T.; Tujunen, N.; Prototopova, V.; Koene, J.; Kordas, K.; Koskinen, J.; Meyyappan, M.; Laurila, T. Integrated Carbon Nanostructures for Detection of Neurotransmitters. *Mol. Neurobiol.* **2015**, *52*, 859–866. [CrossRef]
41. Sanchez-Ferrer, A.; Rodrìguez-Lòpez, J.N.; Garcìa-Cánovas, F.; Garcìa-Camona, F. Tyrosinase: A comprehensive review of its mechanism. *Biochim. Biophys. Acta* **1995**, *1247*, 1–11. [CrossRef]
42. Granero, A.M.; Fernandez, H.; Agostini, E.; Zon, M.L. An amperometric biosensor based on peroxidases from Brassica napus for the determination of the total polyphenolic content in wine and tea samples. *Talanta* **2010**, *83*, 249–255. [CrossRef] [PubMed]
43. Zejli, H.; de Cisneros, H.H.; Naranjo-Rodriguez, I.; Liu, B.; Temsamani, K.R.; Marty, J.L. Phenol biosensor based on Sonogel-Carbon transducer with tyrosinase alumina sol–gel immobilization. *Anal. Chim. Acta* **2008**, *612*, 198–203. [CrossRef]
44. Shiddiky, M.J.A.; Torriero, A.A.J. Application of ionic liquids in electrochemical sensing systems. *Bios. Bioelectron.* **2011**, *26*, 1775–1787. [CrossRef] [PubMed]
45. Petrucci, R.; Pasquali, M.; Scaramuzzo, F.A.; Curulli, A. Recent Advances in Electrochemical Chitosan-Based Chemosensors and Biosensors: Applications in Food Safety. *Chemosensors* **2021**, *9*, 254. [CrossRef]
46. Karrat, A.; Amine, A. Recent advances in chitosan-based electrochemical sensors and biosensors. *Arab. J. Chem. Environ. Res.* **2020**, *7*, 66–93.
47. Fisher, M.J.E. Amine coupling through EDC/NHS: A practical approach. *Methods Mol. Biol.* **2010**, *627*, 55–73.
48. Ducker, R.E.; Montague, M.T.; Leggett, G.J. A comparative investigation of methods for protein immobilization on self-assembled monolayers using glutaraldehyde, carbodiimide, and anhydride reagents. *Biointerphases* **2008**, *3*, 59. [CrossRef]
49. Liu, C.Y.; Chou, Y.C.; Tsai, J.H.; Huang, T.M.; Chen, J.Z.; Yeh, Y.C. Tyrosinase/Chitosan/Reduced Graphene Oxide Modified Screen-Printed Carbon Electrode for Sensitive and Interference-Free Detection of Dopamine. *Appl. Sci.* **2019**, *9*, 622. [CrossRef]
50. Cheng, Y.; Liu, Y.; Huang, J.; Xian, Y.; Zhang, Z.; Jin, L. Fabrication of Tyrosinase Biosensor Based on Multiwalled Carbon Nanotubes-Chitosan Composite and Its Application to Rapid Determination of Coliforms. *Electroanalysis* **2008**, *20*, 1463–1469. [CrossRef]
51. Wan, D.; Yuan, S.; Li, G.L.; Neoh, K.G.; Kang, E.T. Glucose biosensor from covalent Immobilization of Chitosan-Coupled Carbon Nanotubes on Polyaniline-Modified Gold Electrode. *ACS Appl. Mater. Interfaces* **2010**, *2*, 3083–3091. [CrossRef] [PubMed]
52. Lupu, S.; Lete, C.; Cătălin Balaure, P.; Ion Caval, D.; Mihailciuc, C.; Lakard, B.; Hihn, J.Y.; del Campo, F.J. Development of Amperometric Biosensors Based on Nanostructured Tyrosinase-Conducting Polymer Composite Electrodes. *Sensors* **2013**, *13*, 6759–6774. [CrossRef] [PubMed]
53. Gao, Y.; Wu, Y. Recent advances of chitosan-based nanoparticles for biomedical and biotechnological applications. *Int. J. Biol. Macromol.* **2022**, *203*, 379–388. [CrossRef] [PubMed]
54. Wang, J.; Zhuang, S. Chitosan-based materials: Preparation, modification and application. *J. Clean. Prod.* **2022**, *355*, 131825. [CrossRef]
55. Anusha, J.R.; Raj, C.J.; Cho, B.-B.; Fleming, A.T.; Yu, K.-H.; Kim, B.C. Amperometric glucose biosensor based on glucose oxidase immobilized over chitosan nanopartoicles from glaudius of *Uroteuthis duvauceli*. *Sens. Actuators B Chem.* **2015**, *215*, 536–543. [CrossRef]
56. Kim, H.S.; Lee, J.S.; Kim, M.I. Poly-γ-glutamic Acid/Chitosan hydrogel nanoparticles entrapping glucose oxidase and magnetic nanoparticles for glucose biosensing. *J. Nanosci. Nanotechnol.* **2020**, *20*, 5333–5337. [CrossRef]
57. Kalam, M.A. Development of chitosan nanoparticles coated with hyaluronic acid for topical ocular delivery of dexamethasone. *Int. J. Biol. Macromol.* **2016**, *89*, 127–136. [CrossRef]
58. Obaje, E.A.; Cummins, G.; Schulze, H.; Mahmood, S.; Desmulliez, M.P.; Bachmann, T.T. Carbon screen-printed electrodes on ceramic substrates for label-free molecular detection of antibiotic resistance. *J. Interdiscip. Nanomed.* **2016**, *1*, 93–109. [CrossRef]
59. Rampino, A.; Borgogna, M.; Blasi, P.; Bellich, B.; Cesaro, A. Chitosan nanoparticles: Preparation, size evolution, and stability. *Int. J. Pharm.* **2013**, *455*, 219–228. [CrossRef]
60. Oldham, K.B. Analytical expression for the reversible Randles-Sevcik function. *J. Electroanal. Chem. Interfacial Electrochem.* **1979**, *105*, 373–375. [CrossRef]
61. Lavagnini, I.; Antiochia, R.; Magno, F. An extended method for the practical evaluation of the standard rate constant from cyclic voltammetric data. *Electroanalysis* **2004**, *16*, 505–506. [CrossRef]
62. Lavagnini, I.; Antiochia, R.; Magno, F. A calibration-base method for the evaluation of the detection limit of an electrochemical biosensor. *Electroanalysis* **2007**, *19*, 1127–1230. [CrossRef]
63. Marroquin, J.B.; Rhee, K.Y.; Park, S.J. Chitosan nanocomposite films: Enhanced electrical conductivity, thernmal stability, and mechanical properties. *Carbohydr. Polym.* **2013**, *92*, 1783–1791. [CrossRef] [PubMed]
64. Zhang, Z.; Wang, B.Q.; Xu, B.; Cheng, G.J.; Dong, S.J. Amperometric quantification of polar organic solvents based on a tyrosinase biosensor. *Anal. Chem.* **2000**, *72*, 3455–3460. [CrossRef] [PubMed]
65. Cosnier, S.; Popescu, I.C. Poly(amphilic pyrrole)-tyrosinase-peroxidase electrode for amplified flow injection-amperometric detection of phenol. *Anal. Chim. Acta* **1996**, *319*, 145–151. [CrossRef]
66. Kamin, R.A.; Wilson, G.S. Rotating ring-disk enzyme electrode for biocatalysis kinetic studies and characterization of the immobilized enzyme layer. *Anal. Chem.* **1980**, *52*, 1198–1205. [CrossRef]
67. Espin, J.C.; Varon, R.; Fenoll, L.G.; Gilabert, M.A.; Garcia-Ruiz, P.A.; Tudela, J.; Garcia-Canovas, F. Kinetic characterization of the substrate specificity and mechanism of mushroom tyrosinase. *Eur. J. Biochem.* **2000**, *267*, 1270–1279. [CrossRef]

68. Zou, Y.S.; Lou, D.; Dou, K.; He, L.L.; Dong, Y.H.; Wang, S.L. Amperometric tyrosinase biosensor based on boron-doped nanocrystalline diamond film electrode for the detection of phenolic compounds. *J. Solid State Electrochem.* **2016**, *20*, 47–54. [CrossRef]
69. Rahman, S.F.; Min, K.; Park, S.H.; Park, J.H.; Yoo, J.C.; Park, D.H. Highly sensitive and selective dopamine detection by an amperometric biosensor based on tyrosinase/MWNT/GCE. *Korean J. Chem. Eng.* **2016**, *33*, 3442–3447. [CrossRef]
70. Li, H.Q.; Hu, X.; Zhu, H.M.; Zang, Y.; Xue, H.G. Amperometric phenol biosensor based on a new immobilization matrix: Polypyrrole nanotubes derived from methyl orange as dopant. *Int. J. Electrochem. Sci.* **2017**, *12*, 6714–6728. [CrossRef]
71. Sethuraman, V.; Muthuraja, P.; Anandha Raj, J.; Manisankar, P. A highly sensitive electrochemical biosensor for catechol using conducting polymer reduced graphene oxide–metal oxide enzyme modified electrode. *Biosens. Bioelectron.* **2016**, *84*, 112–119. [CrossRef] [PubMed]
72. Vicentini, F.C.; Garcia, L.L.C.; Figueiredo-Filho, L.C.S.; Janegitz, B.C.; Fatibello-Filho, O. A biosensor based on gold nanoparticles, dihexadecylphosphate, and tyrosinase for the determination of catechol in natural water. *Enzym. Microb. Technol.* **2016**, *84*, 17–23. [CrossRef] [PubMed]
73. Araque, E.; Villalonga, R.; Gamella, M.; Martínez-Ruiz, P.; Reviejo, J.; Pingarrón, J.M. Crumpled reduced graphene oxide–polyamidoamine dendrimer hybrid nanoparticles for the preparation of an electrochemical biosensor. *J. Mater. Chem. B* **2013**, *1*, 2289–2296. [CrossRef] [PubMed]
74. Borisova, B.; Ramos, J.; Díez, P.; Sánchez, A.; Parrado, C.; Araque, E.; Villalonga, R.; Pingarrón, J.M. A Layer-by-Layer biosensing architecture based on polyamidoamine dendrimer and carboxymethylcellulose-modified graphene oxide. *Electroanalysis* **2015**, *27*, 2131–2138. [CrossRef]
75. Lete, C.; Lupu, S.; Lakard, B.; Hihn, J.Y.; del Campo, F.J. Multi-analyte determination of dopamine and catechol at single-walled carbon nanotubes—Conducting polymer—Tyrosinase based electrochemical biosensors. *J. Electroanal. Chem.* **2015**, *744*, 53–61. [CrossRef]
76. Min, K.; Yoo, Y.J. Amperometric detection of dopamine based on tyrosinase-SWNTs-Ppy composite electrode. *Talanta* **2009**, *80*, 1007–1011. [CrossRef]
77. Meloni, F.; Spychalska, K.; Zając, D.; Pilo, M.I.; Zucca, A.; Cabaj, J. Application of a Thiadiazole-derivative in a Tyrosinase-based Amperometric Biosensor for Epinephrine Detection. *Electroanalysis* **2021**, *33*, 1639–1645. [CrossRef]